Biosensors and Bioelectronics 102 (2018) 425–431

Contents lists available at ScienceDirect

Biosensors and Bioelectronics

journal homepage: www.elsevier.com/locate/bios

A multi-functional gold/iron-oxide nanoparticle-CNT hybrid nanomaterial as virus DNA sensing platform

Jaewook Lee[a], Masahiro Morita[b], Kenshin Takemura[b], Enoch Y. Park[a,b,*]

[a] Research Institute of Green Science and Technology, Graduate School of Integrated Science and Technology, Shizuoka University, 836 Ohya Suruga-ku, Shizuoka 422-8529, Japan

[b] Department of Applied Biological Chemistry, Graduate School of Integrated Science and Technology, Shizuoka University, 836 Ohya Suruga-ku, Shizuoka 422-8529, Japan

ARTICLE INFO

Keywords:
Electrical resistance biosensor
Binary nanoparticle-decorated carbon nanotubes
DNA detection
Influenza virus
Norovirus
Magnetically deposited sensing channel

ABSTRACT

Nanoparticle (NP)-carbon nanomaterial hybrid structures have garnered significant attention due to their synergistic effects. Based on their interesting properties, hybrid nanomaterial-based sensing platforms have been investigated to achieve high sensitivity and selectivity detection. In our study, binary-NP-decorated carbon nanotubes (bNP-CNTs) were successfully synthesized through a simple two-step method and applied as a biosensing platform. Gold (Au)/iron-oxide magnetic NP-decorated CNTs (Au/MNP-CNT) were used for influenza and norovirus DNA sensing channels. To demonstrate biosensing, first, the Au/MNP-CNTs were magnetically aligned on a Pt-interdigitated electrode, and then, a thiol-group-functionalized probe DNA was attached to the Au NP surface on the bNP-CNT hybrid structure through thiol chemistry. DNA hybridization between the target influenza or norovirus DNA and probe DNA was measured to monitor an electrical conductivity change of the Au/MNP-CNTs. Various concentrations of target DNA from 1 pM to 10 nM were monitored, and the limits of detection for influenza virus and norovirus were calculated to be approximately 8.4 pM and 8.8 pM, respectively. The specificity was confirmed using different mismatched DNA sequences, showing high specificity. Therefore, this Au/MNP-CNT-based DNA sensing system exhibited excellent detection potential, and such hybrid materials could be universally applied as a highly sensitive and selective biosensing system.

1. Introduction

Recently, nanoparticle (NP)-functionalized carbon nanomaterials (CNMs) have attracted significant attention due to their enhanced physical and excellent synergistic properties, for example, surface-enhanced Raman scattering (SERS), magneto optical (MO) effects, plasmonic resonance energy transfer (PRET), enhanced catalytic properties, mechanical properties, and electrical conductivity (Han et al., 2014; Kauffman et al., 2010; Kim et al., 2017b; Klinkova et al., 2014; Lee and Lee, 2017; Lee et al., 2016). Additionally, these hybrid materials have been applied in various fields, such as nano-optics, batteries, nano-electronics, sensors, catalysis, and nano-biology (Baro et al., 2013; Chen et al., 2014; Lee et al., 2015b, 2011b; Narayanan et al., 2012).

Notably, these attractive multi-functionalities of hybrid NP-CNMs were employed as excellent biosensing platforms for public safety and personal well-being (Kim et al., 2016; Liu and Guo, 2012; Myung et al., 2012). In order to prevent the spreading of infectious diseases in public, rapid, high sensitivity and high selectivity sensing systems are required (Ahmed et al., 2017a; Kim et al., 2017a; Wu et al., 2017). Several NP-graphene (NP-GRP) or NP-carbon nanotube (NP-CNT) materials have been developed for biosensing systems with various approaches; for example, colorimetry, fluoro-immunoassays, electrochemical, and electrical resistance monitoring systems (Ahmed et al., 2017b; Lee et al., 2014, 2015a, 2017, 2017c; Yang et al., 2011).

In this study, two kinds of viruses were detected with multi functionalized-CNTs based sensing platform. Firstly, influenza virus A DNA that is well known as highly infectious disease in worldwide was targeted. Depending on the genotype, influenza viruses are classified into genotypes A, B, and C. Influenza virus A is susceptible to mutation in surface proteins and have cause pandemics several times (Christman et al., 2011). On the other hand, norovirus was regarded as another target virus. Only 100 or fewer virus can infect the human body (Kwan et al., 2017). Moreover, a host medium does not exist for a norovirus culture and, therefore, replicating this virus is difficult for biosensing studies (Karst et al., 2014; Orchard et al., 2016). Thus, norovirus DNA was applied for detection performance.

* Corresponding author at: Research Institute of Green Science and Technology, Graduate School of Integrated Science and Technology, Shizuoka University, 836 Ohya Suruga-ku, Shizuoka 422-8529, Japan.
E-mail address: park.enoch@shizuoka.ac.jp (E.Y. Park).

https://doi.org/10.1016/j.bios.2017.11.052
Received 6 September 2017; Received in revised form 15 November 2017; Accepted 16 November 2017
Available online 21 November 2017
0956-5663/

Thus, Influenza virus A (H1N1) and norovirus DNAs detection were demonstrated using Au/magnetic NP-CNT (Au/MNP-CNT) sensing channels. First, Au/MNP-CNTs were prepared in deionized (DI) water through a simple two-step method under ambient conditions (Lee et al., 2015b). Then, Au/MNP-CNTs were aligned on a Pt-interdigitated electrode by an external magnetic field, and after the alignment process, a probe DNA was conjugated on the Au/MNP-CNTs via interactions between the thiol groups in the probe DNA and Au in Au/MNP-CNT (Alivisatos et al., 1996; Liu, 2014; Mirkin et al., 1996). To detect the influenza virus DNA or norovirus DNA, the electrical conductivity of the Au/MNP-CNTs was monitored depending on the hybridization between the target DNA and probe DNA on the Au/MNP-CNT surface under various concentrations.

2. Materials and method

2.1. Materials and instruments

Gold(III) chloride trihydrate (99.9%), gallic acid monohydrate (GA; 3,4,5-trihydroxy benzoic acid monohydrate), ferric chloride, ferrous chloride tetrahydrate, 25% ammonia solution and multi-walled carbon nanotubes (MWCNTs) were purchased from Sigma-Aldrich (Tokyo, Japan). The planar Pt-interdigitated electrode (Pt-IDE) was obtained from Dropsens (Llanera, Spain). Influenza virus DNA, norovirus DNA and zika virus DNA were purchased from Fasmac (Kanagawa, Japan).

The absorbance of the Au/MNP-CNTs to measure the plasmonic properties was analyzed by ultraviolet/visible (UV/Vis) spectroscopy (Infinite® F500, TECAN, Ltd., Männedorf, Switzerland). The chemical functional groups of the MWCNTs and Au/MNP-CNTs were measured by Fourier-transform infrared (FT-IR) spectroscopy (FT-IR 6300, JASCO, Japan). Structural analysis of the Au/MNP-CNTs was performed using powder X-ray diffraction (PXRD) (RINT ULTIMA, Rigaku, Corp., Tokyo, Japan) with Cu Ka radiation and a Ni filter. The diffraction patterns of the Au/MNP-CNTs were collected at a 2 theta range of 20–100° at a scan rate of 0.01° per step and 10 s per point. The Fe and Au element of Au/MNP-CNT were analyzed by using x-ray photoelectron spectroscopy (XPS) with MgKα X-ray (ESCA-3400, Shimadzu, Kyoto, Japan). The magnetic properties of the Au/MNP-CNTs were characterized by a superconducting quantum interference device (SQUID, MPMS-XL7, Quantum Design, Inc., San Diego, CA, USA). The surface morphologies and structures of the MWCNTs and Au/MNP-CNTs were observed by transmission electron microscopy (TEM, JEM-1400, JEOL, Tokyo, Japan) and scanning electron microscopy (SEM, JSM-6510 LV, JEOL, Tokyo, Japan). To demonstrate DNA detection, the electrical conductivity and resistance change of the Au/MNP-CNT sensing channel were monitored using a potentiometer (VersaSTAT 4, AMETEK Inc., Berwyn, PA, USA).

2.2. Preparation of Au/MNP-CNT

To prepare Au/MNP-CNT, first, oxidizable magnetic NPs were synthesized as a reducing agent (Lee and Lee, 2017; Lee et al., 2015b, 2017). Briefly, 2 mmol of ferrous chloride tetrahydrate and 1 mmol of ferric chloride were dissolved in 40 mL of DI water. Then, 1 mL of an ammonia solution (25% w/w) was added into the mixture, and the mixture was stirred for 10 min to form magnetic iron oxide NPs (MNPs). Subsequently, 3 mmol of GA was poured into the MNP solution, and the solution was stirred at 90 °C for 30 min. After the reaction, GA-modified MNPs (GA-MNPs) precipitated and were purified by excess acetone and magnetic separation. Finally, the GA-MNPs were obtained to use as oxidizable MNPs.

The Au/MNP-CNTs were prepared using a simple two-step procedure; 10 mmol of gold(III) chloride trihydrate and 2 mg of MWCNTs were dispersed in DI water (50 mL) by sonication for 30 min. In addition, 1 mL of GA-MNPs were added into the Au^{3+}/CNT mixture and stirred for 3 h. During this process, oxidizable GA-MNPs converted Au ions to Au NPs on the surface of the MWCNTs. In addition, GA-MNPs attached on the surface of the CNTs through < pi > - < pi > interactions between benzene in GA and the CNTs.

2.3. Bioconjugation between functionalized nanomaterials and probe DNA

The Au/MNP-CNTs were aligned and deposited on Pt-IDE by an external magnetic field for utilization as an influenza virus or norovirus DNA sensing channel. Firstly, 15 μL (30 μg) of Au/MNP-CNT solution (2 mg/mL concentration) was dropped on the Pt-IDE. The amount of hybrid material was optimized in our previous research (Lee et al., 2017). After the alignment process, 40 μL of thiol (-SH)-modified probe DNA (100 nM concentration) was added on the Au/MNP-CNT structure and reacted for 1 h at 24 °C to conjugate the Au/MNP-CNT surface with probe DNA. After 1 h, excess DNA was removed by washing three times. The sequence of the probe DNA is described below.

Sequence of the probe DNA for influenza virus: SH-(spacer)-*TTTC AGTTATTATGCCGTTGTATTT*

Sequence of probe DNA for norovirus: SH-(spacer)-TTTTT*AGGACT GTAG*

In this case, the SH-modified probe DNA was attached to the surface of Au NPs through thiol chemistry, and as a result, this structure could serve as a sensing channel for influenza virus or norovirus DNA detection. In addition, simple carbon chain (C6) based spacer was also modified in the probe DNA structure to introduce the sufficient distance from the surface of Au/MNP-CNT to hybridization part with target DNA. The hybridization part for DNA detection is indicated by the blue and red colors in each sequence as shown in the next section.

2.4. Target DNA detection by probe-DNA-modified Au/MNP-CNT-deposited electrode

To demonstrate the influenza virus A (H1N1) DNA and norovirus DNA detection test using the Au/MNP-CNT sensing channel, various concentrations of target DNA and several mismatched DNA sequences were introduced, as shown below:

Target influenza H1N1 virus DNA: *AAATACAACGGCATAATAACT GAAA*

Single mismatched DNA: AAATACAACGTCATAATAACTGAAA

Fully mismatched DNA: TGAAGCTAACCGGTAAGCGCTATAG

Target norovirus DNA: *TCCTGACATC*ATACAAGCTAACTCC

Zika virus DNA: TGCTAAAACGCGGAGTAGCCCGTGT

The sensitivity test of the Au/MNP-CNT sensing channel was conducted from 1 pM to 10 nM concentrations, and the selectivity test was performed with several different types of DNA sequences at a 10 nM concentration. The conductivity of sensing channel was measured from – 0.4–0.4 V to monitor the resistance change depending on the DNA concentrations. And the resistance value was collected from I/V curve in each virus DNA concentration. The response values of the sensitivity and selectivity were estimated by the ratio of the resistance change before and after hybridization using the equation described below (Lee et al., 2017; Tran et al., 2014):

$$\triangle R/R_{pro} = \{R_{(pro+hyb)} - R_{pro}\}/R_{pro} \quad (1)$$

Here, the resistance value (R_{pro}) of the probe DNA-Au/MNP-CNTs was denoted R_0 to evaluate the sensing performance of the hybrid sensing channel. The $R_{(pro+hyb)}$ value indicates the resistance after the probe-target DNA hybridization process on the Au/MNP-CNT sensing channel. The limit of detection (LOD) was confirmed using Equation S1 in the Supporting Information (SI).

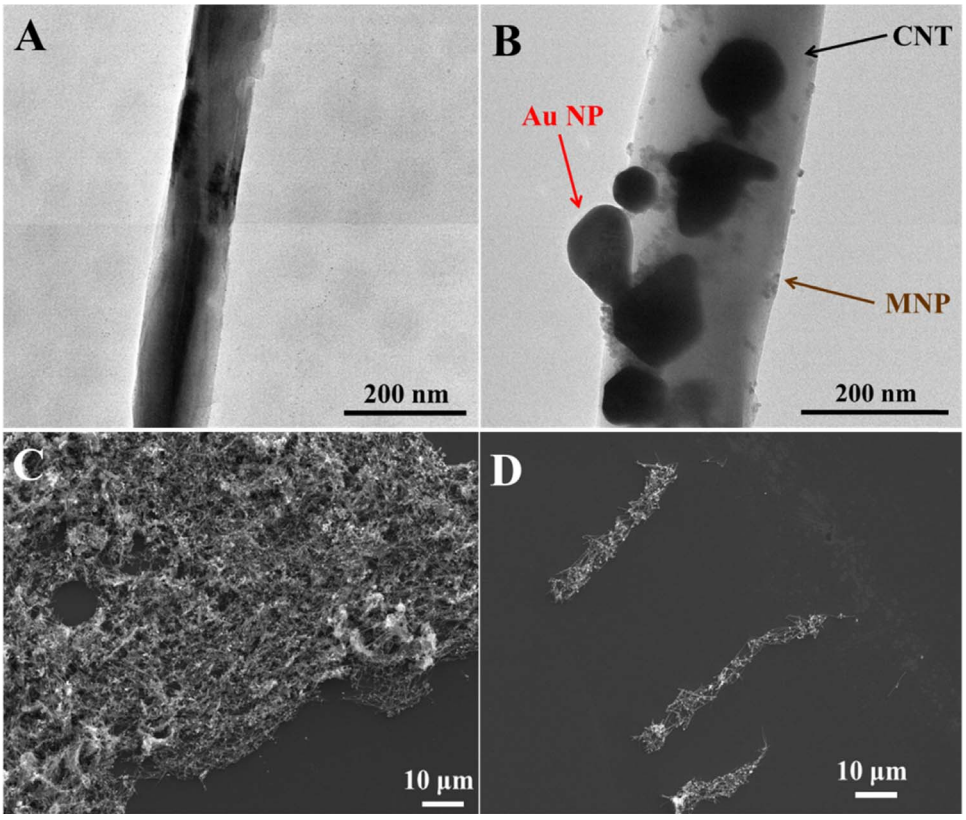

Fig. 1. TEM images of the (A) CNT and (B) Au/MNP-CNT; SEM images of the Au/MNP-CNTs (C) without magnetic alignment and (D) after magnetic alignment.

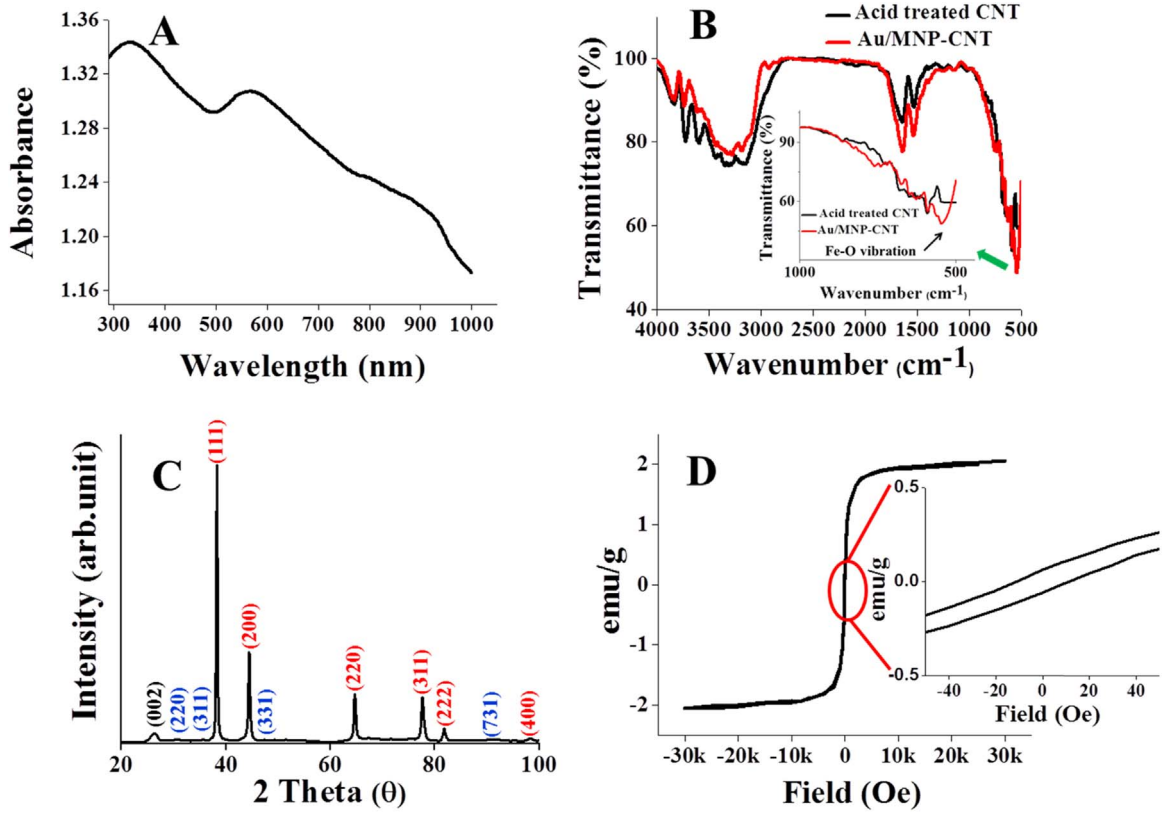

Fig. 2. Physicochemical analysis of the Au/MNP-CNTs. (A) UV/Vis and (B) FT-IR spectra (enlarged spectra was inserted from 500 cm^{-1} to 1000 cm^{-1}) and (C) XRD patterns (black label; MWCNTs, blue label; GA-MNPs and red label; Au NPs); (D) SQUID hysteresis curve of the Au/MNP-CNTs.

3. Results and discussion

3.1. Morphology of Au/MNP-CNTs

The CNT and Au/MNP-decorated CNT surfaces were observed by TEM (Fig. 1A and B). Before modification of the CNTs with NPs, CNTs with clean and smooth surfaces were observed. After the decoration process, two different NPs were observed on the CNT surface: black NPs indicate Au NPs, and gray color dots correspond to GA-MNPs. In addition, these NPs were well dispersed on the CNT surface. Because of the difference of surface electron density between Au NPs and the GA-MNPs, these NPs could be distinguished by their color. In addition, Au NPs were grown using only the reducing agent (oxidizable MNP) without a surface stabilizer, and the size of these NPs were not controlled. As a result, large sizes up to 200 nm could be grown. Generally, to control the size of Au NPs during synthesis step, organic compound based surface stabilizer was used however, that chemical could induce reduction of electrical conductivity of hybrid material and cause other side effect. Also, that chemical stabilizer could prevent the direct binding of probe DNA on Au NPs. In this study, electrical conductivity is a key factor to detect a target virus DNA via hybridization process. Thus, any surface stabilizer for Au NP was not introduced to control the size. On the other hand, blurred black Au NPs were observed, which likely corresponded to NPs grown on the back side of the CNT. The size of GA-MNP was observed by TEM and it was around 12 nm. The magnetically aligned hybrid CNTs were observed by SEM. Without an external magnetic field, the Au/MNP-CNTs were randomly deposited on the Si wafer (Fig. 1C). However, several lines of bundles of hybrid CNTs were observed, which establishes that the Au/MNP-CNTs were magnetically aligned on the Si wafer by an external magnetic field (Fig. 1D). Thus, this hybrid carbon nanomaterial would be aligned on the Pt-IDE surface for application as a DNA sensing channel.

3.2. Physicochemical properties of Au/MNP-CNTs

The physicochemical characteristics of the Au/MNP-CNTs are shown in Fig. 2. First, the surface plasmon properties of the Au/MNP-CNTs were measured by UV/Vis spectroscopy. A broadened absorbance band was measured with a λ_{max} of 600 nm (Fig. 2A). From the TEM image, the morphology of the Au NPs were not homogeneous, with sizes varying from 20 nm to 200 nm (Lee et al., 2011a). These results indicate that the plasmonic absorbance range of the Au NPs would be slightly wide, which agrees well with the TEM image. On the other hand, at wavelengths over 700 nm, the plasmonic coupling effect between closely located Au NPs on the CNTs was analyzed. In this case, because the CNTs possess < pi > electrons, Au NP surface plasmon could have interacted with each other, and as a result, longitudinal plasmonic coupling between the Au NPs occurred at the CNT surface. The functional groups of the Au/MNP-CNTs were characterized by FT-IR spectroscopy. The FT-IR spectrum of Au/MNP-CNT shown in Fig. 2B exhibits a band at 550 cm^{-1}, corresponding to the Fe-O stretching band. The aromatic region of the Au/MNP-CNTs was indicated at approximately 1510 cm^{-1}, which matched well with the vibration spectrum of the aromatic bonds of acid-treated CNTs (black spectrum). This indicates that the CNT structure was not considerable changed after decoration. The peak at approximately 1651 cm^{-1} corresponded to the C=O vibration mode of acid treated CNT and Au/MNP-CNT. On the other hand, GA on the surface of MNP was composed with hydroxyl groups, carboxyl group and benzene, so it meant that functional group region of FT-IR spectrum of GA was overlapped with acid treated CNT. The lattice structure of the Au/MNP-CNTs was analyzed by PXRD, as shown in Fig. 2C. At 2 theta = 26.29° in the XRD pattern, the (002) plane of the acid-treated MWCNTs was observed (ICSD card no: 01-075-1621). On the other hand, several diffraction patterns of Au NPs with (111), (200), (220; red), (311), (222), and (400) planes were analyzed at 2 theta = 38.31°, 44.43°, 64.51°, 77.71°, 81.80°, and 98.24°, respectively (ICSD card no: 00−004−0784). In addition, the XRD pattern of the GA-MNPs was analyzed, displaying (220; blue), (311), (331) and (731) planes identified at 2 theta = 30.63°, 35.25°, 47.18°, and 89.67°, respectively (JCPDS card no: 79–0417). The chemical components of Au/MNP-CNT were also characterized by using XPS. In this case, Fe 2p orbital spectrum was observed between 700 eV and 740 eV. According to supplementary Fig. S1A (Fig S1A), Fe $2p_{2/3}$ band was observed around 710.7 eV and Fe $2P_{1/3}$ was indicated about 725 eV. In addition, Au 4 f orbital spectrum was also shown from 80 eV to 93 eV and Au 4 $f_{5/2}$ and Au 4 $f_{7/2}$ was indicated at 86.9 eV and 83.2 eV, respectively (Fig S1B). The magnetic properties of the Au/MNP-CNTs were analyzed using a SQUID at room temperature from –30 kOe to 30 kOe. A nonlinear magnetic − hysteresis relationship and a reversible hysteresis loop were observed for the Au/MNP-CNTs (Fig. 2D). The coercive force of the Au/MNP-CNTs was measured to be approximately − 10 Oe and 10 Oe. On the other hand, remanence effects of approximately 0.06 and − 0.06 emu/g were indicated for the Au/MNP-CNTs. According to this hysteresis loop, the CNT structure exhibited magnetic properties after hybridization with the GA-MNPs. Additionally, this indicates that the Au/MNP-CNTs were aligned on the electrode under an external magnetic field.

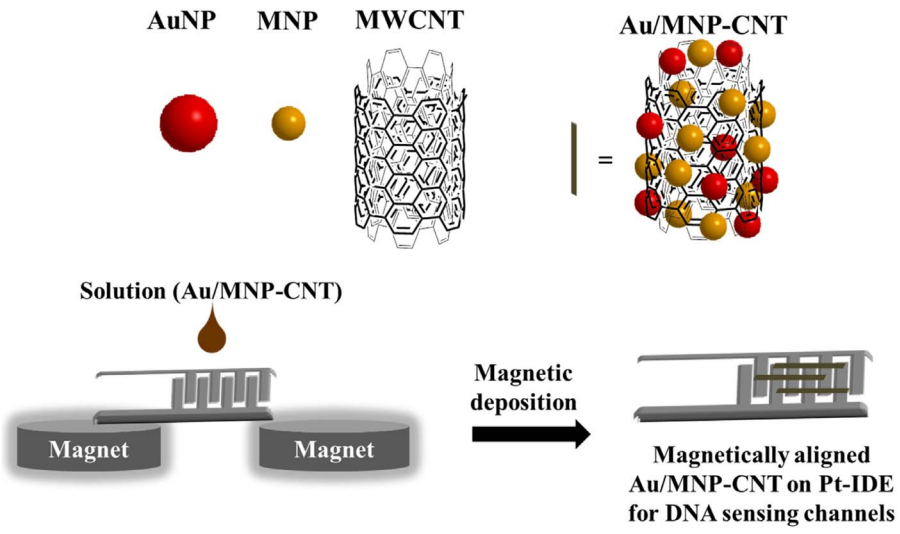

Fig. 3. Illustration of the preparation of the magnetically aligned Au/MNP-CNTs on the Pt-IDE for DNA sensing channels (not to scale).

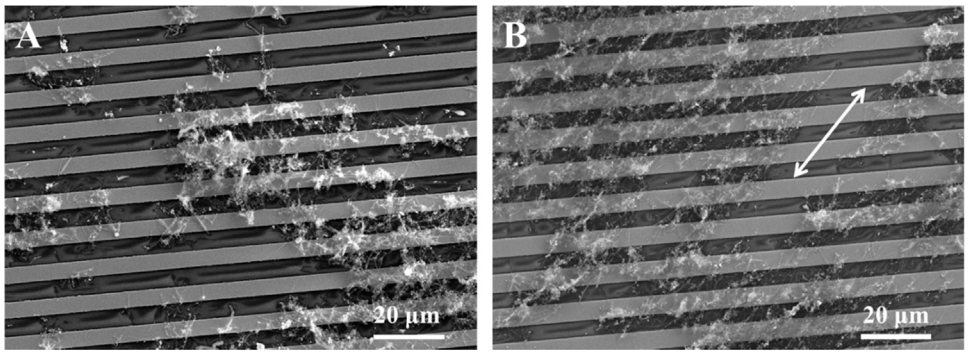

Fig. 4. SEM images of the Au/MNP-CNTs on the Pt-IDE (A) without magnetic alignment and (B) after magnetic alignment.

3.3. Fabrication of Au/MNP-CNTs based biosensing platform

The preparation process of the Au/MNP-CNT sensing channel is illustrated in Fig. 3. First, the Pt-IDE was placed between two magnets to generate a magnetic field. Then, the Au/MNP-CNT solution was dropped onto the Pt-IDE and dried under room temperature under atmospheric conditions. The Au/MNP-CNTs were aligned on the Pt-IDE during solvent evaporation due to the external magnetic field without any soft or hard template. After alignment, the structures of the Au/MNP-CNTs were observed by SEM. In our previous study, Au/MNP-graphenes (GRPs) were utilized as sensing channels to detect norovirus like particle (Lee et al., 2017). In that case, hybrid GRPs were magnetically stacked, but in this study, Au/MNP-CNT was directly aligned on the Pt-IDE. It meant that electron pass way of hybrid CNT on the electrode was shorter than that of hybrid GRP. Thus, in this work, Au/MNP-CNT was regarded as suitable sensing channel DNA detection.

To demonstrate influenza virus A (H1N1) DNA and norovirus DNA detection using the Au/MNP-CNT sensing channel, this hybrid material was deposited and aligned on the Pt-IDE via magnetic deposition. According to the SEM image in Fig. 4A, without a magnetic field, the Au/MNP-CNTs were randomly located on the Pt-IDE. Moreover, the Au/MNP-CNTs accumulated on certain parts and did not spread out on the Pt-IDE. However, after magnetic deposition, the Au/MNP-CNTs were aligned under the magnetic field. In addition, these hybrid nanomaterials were well dispersed and spread out on the Pt-IDE surface (Fig. 4B). Since the sensing channel behavior could be influenced through the dispersity of conductive materials on the electrode (Lee et al., 2017; Tran et al., 2014), in our case, probe DNA was modified after the alignment process of Au/MNP-CNTs on the Pt-IDE to achieve a DNA sensing system.

3.4. Virus DNA detection with Au/MNP-CNTs sensing channels

Influenza virus DNA detection was conducted with the aligned Au/MNP-CNT sensing platform (Fig. 5A). It is well known that carbon nanomaterials possess good electrical conductivity. But in our previous study, it was established that the conductivity of Au NP decorated graphene (Au-GRP) was poor than that of Au/MNP-CNT, in that case, the resistance of Au-GRP was around 5 kΩ (Lee et al., 2014). Thus, we have selected Au/MNP-CNT as suitable DNA sensing channel for the present investigation. The electrical conductivity of the probe-DNA-modified Au/MNP-CNTs could alter depending on the presence of target DNA. The electrical resistance of the Au/MNP-CNTs increased after DNA hybridization between the probe DNA and target DNA (Fig. 5B). Based on this approach, a sensitivity test of the Au/MNP-CNT-based sensing platform was demonstrated depending on several concentrations of target DNA from 1 pM to 10 nM (Fig. 5C). Before and after the hybridization process, the response values for influenza DNA detection were evaluated via Eq. (1). As the target DNA concentration increased, the resistance difference linearly increased as well. In Fig. 5C, a calibration curve for the target DNA is shown, and its detection limit was calculated as 8.4 pM according to the linear regression from supplementary equation S1.

Recently, several detection methods based on nanotechnology have been introduced to detect several types of virus DNA; the sensing platforms and detection limitations are exhibited in Table 1 and compared with our results. In general, the electrical-signal-based sensing system showed reliable and highly sensitive detection. The selectivity test was performed with several mismatched DNA sequences under 10 nM of DNA and is shown in Fig. 5D. A high response was measured for the target DNA. On the other hand, resistance changes for the single sequence mismatched DNA and fully mismatched DNA were not clearly observed, indicating that the Au/MNP-CNT-based DNA sensing system possesses high selectivity. The alignment effect of the Au/MNP-CNTs for sensing behavior was confirmed by comparing the non-aligned sensing channel and aligned sensing channel at 10 nM DNA. For the magnetically aligned Au/MNP-CNTs, the sensing performance was much better than that of the non-aligned platform (Fig S2).

In addition, norovirus DNA was also monitored using the Au/MNP-CNT sensing channel (Fig. 6). The probe DNA for norovirus DNA was modified on the Au/MNP-CNTs after the alignment process, and the resistance change tendency after hybridization with the target norovirus DNA coincided with the behavior observed for the influenza virus. As the norovirus DNA concentration was increased, the resistance of the sensing channel also increased, and its response linearly changed with the concentration (Fig. 6A). Using supplementary equation S1, the LOD was also estimated to be approximately 8.8 pM Moreover, a selectivity test of this system was performed using several different types of DNA, i.e., 10 nM influenza virus DNA and zika virus DNA. According to Fig. 6B, this system only responded to norovirus DNA, showing excellent selectivity against different DNA disease types.

4. Conclusion

Hybrid Au/MNP-CNTs were simply prepared through a two-step method under ambient and mild conditions. This multi-functional nanomaterial possessed magnetic properties and excellent electrical conductivity. Based on these properties, this hybrid nanostructure was magnetically aligned on the surface of a Pt-IDE and was utilized as a biosensing channel to read an electrical resistance depending on the target DNA. First, influenza virus DNA detection was conducted with the probe-DNA-modified Au/MNP-CNT sensing platform and its detection limitation was estimated to be approximately 8.4 pM Moreover, high specificity of the Au/MNP-CNT-based sensing system was exhibited against several mismatched DNA structures. Subsequently, norovirus DNA was also successfully monitored by the Au/MNP-CNT sensing channel with high sensitivity and selectivity, displaying a LOD of approximately 8.8 pM The multi-functional Au/MNP-CNTs showed excellent DNA sensing performance for different diseases, indicating that this Au/MNP-CNT-based sensing channel could be a universal detection system for various types of DNA through surface modification with specific probe DNA. Therefore, the Au/MNP-CNT-based sensing

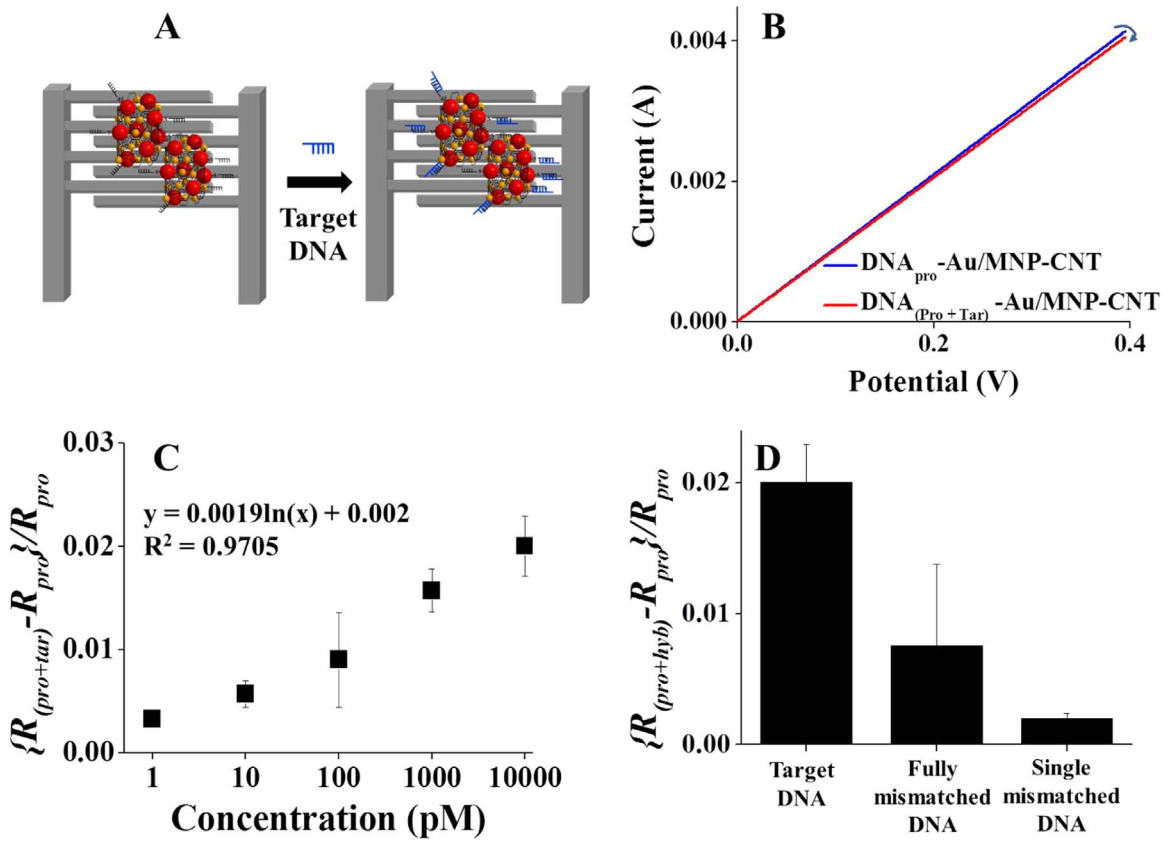

Fig. 5. (A) Illustration of the DNA detection process with hybrid materials (not to scale); (B) IV curve change via hybridization; (C) resistance difference ({$R_{(pro+tar)} - R_{pro}$}/ R_{pro}) for the influenza virus DNA sensitivity test; (D) selectivity test with different types of DNA.

Table 1
Recent research comparison of DNA detection with various approaches.

Detection method	Target virus DNA	LOD	Ref
Field effect transistor with Si nanowires	H1N1	40 pM	(Karnaushenko et al., 2015)
Electrochemical impedance spectroscopy with tubular nanomembrane	H1N1	20 a.M.	(Medina-Sánchez et al., 2016)
Chemiresistor with N-doped MWCNTs	H5N1	20 pM	(Fu et al., 2017)
Linear sweep voltammetry with NP-functionalized MWCNTs	H1N1	8.4 pM	This work
	Norovirus	8.8 pM	This work

platform could be a potential candidate for a highly sensitive and selective detection system in various fields.

Acknowledgments

All the authors appreciate Dr. Chika Nozaki Kato for allowing access to the potentiostat (VeraSTAT 4). This research was supported by the Japan Society for the Promotion of Science (JSPS) Postdoctoral Fellowship for Overseas Researcher (16F16361).

Conflict of interest

The authors declare no competing financial interest.

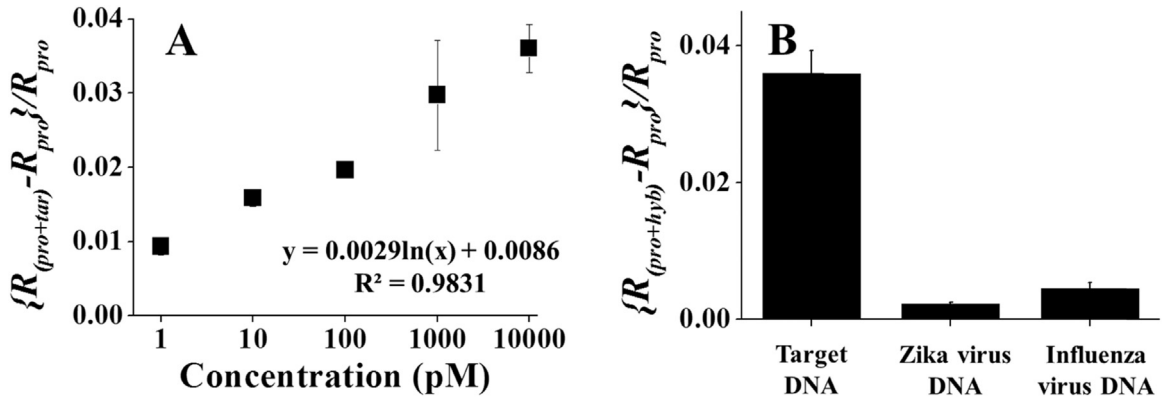

Fig. 6. Norovirus DNA detection with the Au/MNP-CNT sensing channel: (A) sensitivity performance and (B) specificity test.

Appendix A. Supporting information

Supplementary data associated with this article can be found in the online version at http://dx.doi.org/10.1016/j.bios.2017.11.052.

References

Ahmed, S.R., Kim, J., Tran, V.T., Suzuki, T., Neethirajan, S., Lee, J., Park, E.Y., 2017a. In situ self-assembly of gold nanoparticles on hydrophilic and hydrophobic substrates for influenza virus-sensing platform. Sci. Rep. 7, 44495.

Ahmed, S.R., Takemeura, K., Li, T.-C., Kitamoto, N., Tanaka, T., Suzuki, T., Park, E.Y., 2017b. Size-controlled preparation of peroxidase-like graphene-gold nanoparticle hybrids for the visible detection of norovirus-like particles. Biosens. Bioelectron. 87, 558–565.

Alivisatos, A.P., Johnsson, K.P., Peng, X., Wilson, T.E., Loweth, C.J., Bruchez, M.P., Schultz, P.G., 1996. Organization of 'nanocrystal molecules' using DNA. Nature 382 (6592), 609–611.

Baro, M., Nayak, P., Baby, T.T., Ramaprabhu, S., 2013. Green approach for the large-scale synthesis of metal/metal oxide nanoparticle decorated multiwalled carbon nanotubes. J. Mater. Chem. A 1 (3), 482–486.

Chen, X., Cai, Z., Chen, X., Oyama, M., 2014. Synthesis of bimetallic PtPd nanocubes on graphene with N,N-dimethylformamide and their direct use for methanol electrocatalytic oxidation. Carbon 66, 387–394.

Christman, M.C., Kedwaii, A., Xu, J., Donis, R.O., Lu, G., 2011. Pandemic (H1N1) 2009 virus revisited: an evolutionary retrospective. Infect. Genet. Evol. 11 (5), 803–811.

Fu, Y., Romay, V., Liu, Y., Ibarlucea, B., Baraban, L., Khavrus, V., Oswald, S., Bachmatiuk, A., Ibrahim, I., Rümmeli, M., Gemming, T., Bezugly, V., Cuniberti, G., 2017. Chemiresistive biosensors based on carbon nanotubes for label-free detection of DNA sequences derived from avian influenza virus H5N1. Sens. Actuators B: Chem. 249, 691–699.

Han, Z.J., Seo, D.H., Yick, S., Chen, J.H., 2014. MnOx/carbon nanotube/reduced graphene oxide nanohybrids as high-performance supercapacitor electrodes. NPG Asia Mater. 6, e140.

Karnaushenko, D., Ibarlucea, B., Lee, S., Lin, G., Baraban, L., Pregl, S., Melzer, M., Makarov, D., Weber, W.M., Mikolajick, T., Schmidt, O.G., Cuniberti, G., 2015. Light weight and flexible high-performance diagnostic platform. Adv. Healthc. Mater. 4 (10), 1517–1525.

Karst, Stephanie M., Wobus, Christiane E., Goodfellow, Ian G., Green, Kim Y., Virgin, Herbert W., 2014. Advances in norovirus biology. Cell Host Microbe 15 (6), 668–680.

Kauffman, D.R., Sorescu, D.C., Schofield, D.P., Allen, B.L., Jordan, K.D., Star, A., 2010. Understanding the sensor response of metal-decorated carbon nanotubes. Nano Lett. 10 (3), 958–963.

Kim, J., Lee, K.-S., Kim, E.B., Paik, S., Chang, C.L., Park, T.J., Kim, H.-J., Lee, J., 2017a. Early detection of the growth of Mycobacterium tuberculosis using magnetophoretic immunoassay in liquid culture. Biosens. Bioelectron. 96, 68–76.

Kim, J.E., Choi, J.H., Colas, M., Kim, D.H., Lee, H., 2016. Gold-based hybrid nanomaterials for biosensing and molecular diagnostic applications. Biosens. Bioelectron. 80, 543–559.

Kim, Y.-K., Ok, G., Choi, S.-W., Jang, H., Min, D.-H., 2017b. The interfacing structural effect of Ag/graphene oxide nanohybrid films on surface enhanced Raman scattering. Nanoscale 9 (18), 5872–5878.

Klinkova, A., Choueiri, R.M., Kumacheva, E., 2014. Self-assembled plasmonic nanostructures. Chem. Soc. Rev. 43 (11), 3976–3991.

Kwan, H.S., Chan, P.K.S., Chan, M.C.W., 2017. Chapter 2 - Overview of Norovirus as a Foodborne Pathogen. The Norovirus. Academic Press, pp. 21–30.

Lee, J., Ahmed, S.R., Oh, S., Kim, J., Suzuki, T., Parmar, K., Park, S.S., Lee, J., Park, E.Y., 2015a. A plasmon-assisted fluoro-immunoassay using gold nanoparticle-Decorated carbon Nanotubes for monitoring the influenza virus. Biosens. Bioelectron. 64, 311–317.

Lee, J., Mulmi, S., Thangadurai, V., Park, S.S., 2015b. Magnetically aligned iron oxide/gold nanoparticles decorated carbon nanotube hybrid structure as humidity sensor. ACS Appl. Mater. Interfaces 7, 15506–15513.

Lee, J., Kim, J., Ahmed, S.R., Zhou, H., Kim, J.-M., Lee, J., 2014. Plasmon-induced photoluminescence immunoassay for tuberculosis monitoring using gold nanoparticles decorated graphene. ACS Appl. Mater. Interfaces 6, 21380–21388.

Lee, J., Lee, J., 2017. Magneto-optically active magnetoplasmonic graphene. Chem. Commun. 53 (43), 5814–5817.

Lee, J., Lee, K., Park, S., 2016. Environmentally friendly preparation of nanoparticle-decorated carbon nanotube or graphene hybrid structures and their potential applications. J. Mater. Sci. 51, 2761–2770.

Lee, J., Takemura, K., Kato, C.N., Suzuki, T., Park, E.Y., 2017a. Binary nanoparticle graphene hybrid structure-based highly sensitive biosensing platform for norovirus-Like particle detection. ACS Appl. Mater. Interfaces 9 (32), 27298–27304.

Lee, J., Takemura, K., Kato, C.N., Suzuki, T., Park, E.Y., 2017b. Binary nanoparticle-graphene hybrid structure-based highly sensitive biosensing platform for norovirus-like particle detection. ACS Appl. Mater. Interfaces.

Lee, J., Takemura, K., Park, E., 2017c. Plasmonic nanomaterial-based optical biosensing platforms for virus detection. Sensors 17 (10), 2332.

Lee, J., Zhou, H., Lee, J., 2011a. Small molecule induced self-assembly of Au nanoparticles. J. Mater. Chem. 21 (42), 16935.

Lee, J.S., Kwon, O.S., Park, S.J., Park, E.Y., You, S.A., Yoon, H., Jang, J., 2011b. Fabrication of ultrafine metal-oxide-decorated carbon nanofibers for DMMP sensor application. ACS Nano 5 (10), 7992–8001.

Liu, J., 2014. DNA-stabilized, fluorescent, metal nanoclusters for biosensor development. TrAC Trends Anal. Chem. 58, 99–111.

Liu, S., Guo, X., 2012. Carbon nanomaterials field-effect-transistor-based biosensors. NPG Asia Mater. 4 (8), e23.

Medina-Sánchez, M., Ibarlucea, B., Pérez, N., Karnaushenko, D.D., Weiz, S.M., Baraban, L., Cuniberti, G., Schmidt, O.G., 2016. High-performance three-dimensional tubular nanomembrane sensor for DNA detection. Nano Lett. 16 (7), 4288–4296.

Mirkin, C.A., Letsinger, R.L., Mucic, R.C., Storhoff, J.J., 1996. A DNA-based method for rationally assembling nanoparticles into macroscopic materials. Nature 382 (6592), 607–609.

Myung, S., Yin, P.T., Kim, C., Park, J., Solanki, A., Reyes, P.I., Lu, Y., Kim, K.S., Lee, K.-B., 2012. Label-free polypeptide-based enzyme detection using a graphene-nanoparticle hybrid sensor. Adv. Mater. 24 (45), 6081–6087.

Narayanan, R., Deepa, M., Srivastava, A.K., 2012. Nanoscale connectivity in a TiO 2/CdSe quantum dots/functionalized graphene oxide nanosheets/Au nanoparticles composite for enhanced photoelectrochemical solar cell performance. Phys. Chem. Chem. Phys. 14 (2), 767–778.

Orchard, R.C., Wilen, C.B., Doench, J.G., Baldridge, M.T., McCune, B.T., Lee, Y.-C.J., Lee, S., Pruett-Miller, S.M., Nelson, C.A., Fremont, D.H., Virgin, H.W., 2016. Discovery of a proteinaceous cellular receptor for a norovirus. Science.

Tran, V.T., Zhou, H., Kim, S., Lee, J., Kim, J., Zou, F., Kim, J., Park, J.Y., Lee, J., 2014. Self-assembled magnetoplasmonic nanochain for DNA sensing. Sens. Actuators B: Chem. 203, 817–823.

Wu, L., Ji, H., Guan, Y., Ran, X., Ren, J., Qu, X., 2017. A graphene-based chemical nose/tongue approach for the identification of normal, cancerous and circulating tumor cells. NPG Asia Mater. 9 (3), e356.

Yang, M., Choi, B.G., Park, T.J., Heo, N.S., Hong, W.H., Lee, S.Y., 2011. Site-specific immobilization of gold binding polypeptide on gold nanoparticle-coated graphene sheet for biosensor application. Nanoscale 3 (7), 2950–2956.